

Iranian Journal of Oil & Gas Science and Technology, Vol. 12 (2023), No. 4, pp. 1–22
<http://ijogst.put.ac.ir>

Extending CO₂–Oil Relative Permeability Determination Based on Pore-Scale Simulation Using a Phase-Field Approach for Real Porous Media with Nonconstant Fluid Properties

Mohsen Masihi^{1*} and Hasti Firoozmand¹

¹ Department of Chemical and Petroleum Engineering, Sharif University of Technology, Tehran, Iran

Highlights

- Steady-state pore-scale simulations using the phase-field approach are employed to determine CO₂–oil relative permeabilities.
- Simulations are performed on realistic porous media extracted from micro-CT images.
- Nonconstant fluid viscosity and density are considered to represent realistic flow conditions.
- The influence of wetting properties is taken into account.
- The effects of hysteresis on relative permeability behavior are also investigated.

Received: February 17, 2024; revised: April 05, 2025; accepted: April 29, 2025

Abstract

Experimental analysis and numerical simulation of CO₂ injection in oil and gas reservoirs are essential for CO₂ sequestration and enhanced oil recovery applications. However, experimental approaches are often expensive and time-consuming, while numerical methods require input parameters such as two-phase relative permeabilities. In this study, two-phase flow simulations are conducted using a numerical solver based on the phase-field approach under steady-state conditions to determine relative permeability curves. Specifically, flow simulations are performed in realistic porous media, and nonconstant fluid viscosity and density are incorporated, addressing limitations of previous studies. Therefore, the main contribution of this work is the determination of CO₂–oil relative permeabilities in realistic porous media extracted from micro-CT images under conditions of variable fluid viscosity and density. In addition, the influences of wetting properties and hysteresis on relative permeability behavior are investigated.

The numerical results indicate that increased wettability toward the injected fluid enhances displacement efficiency by shifting the intersection point of the relative permeability curves to the right, leading to higher oil recovery, particularly at larger contact angles corresponding to non-wetting conditions and at lower surface tensions. Furthermore, the separation between imbibition and drainage relative permeability curves, representing hysteresis effects, becomes more pronounced as wettability shifts toward larger contact angles. These findings demonstrate the capability of steady-state pore-scale simulations based on the phase-field approach to reliably determine CO₂–oil relative permeability curves when realistic porous media and nonconstant fluid properties are considered.

Keywords: Relative permeability, Pore-scale simulation, Phase field, CO₂ injection, COMSOL

How to cite this article

Masihi, M. and Firoozmand, H., Extending CO₂–Oil Relative Permeability Determination Based on Pore-Scale Simulation Using a Phase-Field Approach for Real Porous Media with Nonconstant Fluid Properties, Iran J. Oil Gas Sci. Technol., Vol. 12, No. 4, p. 1–22, 2023. DOI: [10.22050/ijogst.2025.444342.1704](https://doi.org/10.22050/ijogst.2025.444342.1704)

* Corresponding author:
Email: masihi@sharif.edu

1. Introduction

Nowadays, CO₂ is recognized as one of the most significant pollutant gases and plays a harmful role in the environment. Moreover, trends in fossil fuel consumption, including coal, oil, and gas, over recent decades indicate increasing emissions of this gas. Consequently, projects aimed at geological storage of CO₂ or its utilization for enhanced oil recovery represent effective mitigation solutions. Carbon capture and sequestration (CCS) from various sources, such as power plants, is an efficient method for reducing the concentration of CO₂ in the Earth's atmosphere. One of the primary objectives of sequestration is to confine the gas within deep geological sedimentary formations that possess sufficient storage capacity and caprock integrity, as reported by Ajayi et al. 2019. Potential candidates for CO₂ sequestration include deep saline aquifers, oil and gas reservoirs, and other formations such as coal beds and oil shales, as discussed by Kaldi et al. 2009. Oil and gas reservoirs are particularly attractive targets because they allow for the simultaneous implementation of CO₂ sequestration and enhanced hydrocarbon recovery, as noted by Lokhorst and Wildenborg 2005. In such cases, the availability of existing infrastructure, drilled wells, and surface facilities can substantially reduce project implementation costs.

Several mechanisms are associated with CO₂ sequestration, including oil viscosity reduction, fluid swelling, and changes in fluid density, which occur over different time scales. The interactions among these mechanisms are highly complex because they evolve over time and depend on both the sedimentary environment and the injection process itself, as described by Ajayi et al. 2019. For enhanced oil recovery applications, various CO₂ injection scenarios may be considered, including miscible gas injection under single-contact or multi-contact conditions, immiscible gas injection, near-miscible injection depending on reservoir pressure and temperature, and alternating gas and water injection schemes, as reported by Alvarado et al. 2010, Manrique et al. 2007, and Christensen et al. 2001. Through pressure maintenance, oil viscosity reduction, fluid swelling, density variation, wettability alteration, and changes in interfacial tension, CO₂ injection can modify the relative magnitudes of capillary, viscous, and gravitational forces that govern displacement efficiency and ultimate oil recovery, as discussed by Srivastava et al. 2000, Ghedan 2020, Teklu et al. 2016, and Masihi et al. 2024. For example, Zhang et al. 2011 demonstrated that at low injection rates, the displacement regime transitions from capillary fingering to viscous fingering. In another study, Shi et al. 2016 examined the effects of viscosity, gravity, and wettability on flow behavior in heterogeneous porous media, with particular emphasis on interfacial tension and medium permeability. Furthermore, Hu et al. 2017 investigated wettability effects on CO₂-brine immiscible displacement in geological carbon sequestration using a high-pressure micromodel-microscopy system. Li et al. 2022 conducted CO₂ flooding experiments using three different core samples and analyzed the effects of pore structure and injection pressure on oil recovery, reporting enhanced recovery from small pores with increasing injection pressure. In addition, Hemmati-Sarapardeh et al. 2016 emphasized the role of CO₂ impurities in determining the minimum miscibility pressure. Investigating the trapping of phases during CO₂ injection in porous media is also critical for optimizing enhanced oil recovery and sequestration processes and for assessing reservoir integrity, as highlighted by Herring et al. 2013.

The simultaneous flow of CO₂ and oil within reservoir rocks exhibits complex behavior governed by the relative magnitudes of capillary, viscous, and gravitational forces. These forces control fluid movement and fluid-rock interactions and can result in significant oil trapping. Therefore, modeling two-phase displacement processes, particularly at the pore scale, is essential for effective reservoir management, optimal process design, and safe CO₂ sequestration, as noted by Blunt et al. 2017. The structural complexity of porous media at the pore scale, sedimentary rock heterogeneity, fluid-solid interactions, and dynamic changes in fluid interface morphology pose significant challenges for

multiphase flow simulation, as reported by Ferrari et al. 2015 and Sarraf et al. 2021. Song et al. 2023 reported that the patterns of residual fluid trapping after CO₂ breakthrough depend strongly on wettability, with pore-cluster and blind-end trapping mechanisms predominantly observed in non-oil-wet pores. Spiteri et al. 2005 investigated the role of CO₂ trapping in relative permeability models used to predict the distribution and mobility of CO₂ within geological formations.

The first step in pore-scale flow modeling is the construction of an accurate static model that describes the internal pore structure, including pore connectivity, pore and throat size distributions, surface roughness, and fracture networks. Advances in two-dimensional and three-dimensional micro-CT imaging, combined with image analysis techniques, now enable realistic characterization of internal core structures, thereby improving the representation of pore-scale flow dynamics, as demonstrated by Piri et al. 2005, Wildenschild et al. 2002, and Flannery et al. 1987. For instance, Øren et al. 2019 obtained in situ pore-scale images of CO₂-brine distributions within reservoir samples during low capillary number drainage and imbibition experiments and analyzed the effects of advancing contact angle on capillary trapping. Despite these advances, significant challenges remain in pore-scale modeling, including the upscaling of pore-scale results to the reservoir scale, accurate representation of rock internal geometry, and integration of data across multiple types and spatial scales, as discussed by Blunt et al. 2002 and Kumar et al. 2010.

2. Modeling two-phase flow at the pore scale

Modeling multiphase flow at the pore scale requires appropriate consideration of the underlying displacement physics. Pore-scale simulation methods generally include direct numerical simulation (DNS) and pore network modeling (PNM). In the direct numerical simulation approach, the pore space is first characterized based on micro-CT images, after which an appropriate mesh is generated and the governing flow equations that capture the displacement physics are applied, as described by Basirat et al. 2017. In general, two sets of equations are required: one set describes the bulk flow, and the other captures the interface between the two fluid phases within the porous medium. The Navier–Stokes equations govern the bulk flow behavior, while the fluid–fluid interface is modeled using different formulations such as the volume of fluid, level set, or phase-field methods, as reported by Raeini et al. 2012, Sethian et al. 2003, and Akhlaghi et al. 2014.

An alternative approach for pore-scale flow simulation is pore network modeling. This method represents the complex pore structure of the medium as a network of pores and throats, on which the flow equations are solved numerically. Although pore network models are computationally efficient, they typically rely on several simplifying assumptions that can reduce the accuracy of the results, as discussed by Sethian et al. 2003, Akhlaghi et al. 2014, and Joekar-Niasar et al. 2010. In direct numerical simulation, one set of equations, such as the Navier–Stokes equations, describes the motion of the bulk phases, while another set of equations tracks the evolution of the fluid–fluid interface, as noted by Ferrari et al. 2015 and Basirat et al. 2017. These equations are commonly implemented using finite element, finite volume, or boundary element methods with either structured or adaptive meshes. Solving the governing equations yields the spatial distributions of velocity, pressure, and phase saturation, as well as the evolution of the fluid interface during two-phase displacement, as reported by Raeini et al. 2012 and Yue et al. 2006.

One approach for tracking the fluid–fluid interface is the moving mesh method. In this Lagrangian-based algorithm, the mesh configuration evolves with the flow field, as described by Hu et al. 2001 and Huang 1994. Another interface-tracking technique is the front-tracking method, which explicitly represents the interface using marker points or meshes, as discussed by Tryggvason et al. 2001 and Popinet et al. 1999. However, front-tracking methods face challenges in accurately identifying and

maintaining the interface in geometrically complex porous structures, as reported by Meakin et al. 2009 and Sethian et al. 2003.

Eulerian interface-capturing methods provide another class of techniques for modeling fluid interfaces. Examples include the volume of fluid, level set, and phase-field methods, as described by Hirt et al. 1981 and Sussman 1994. Although the volume of fluid method ensures mass conservation, it may fail to accurately capture interface curvature in certain situations. In this approach, discontinuities in fluid properties across the interface can introduce numerical disturbances, and wetting boundary conditions, such as nonequilibrium contact angle formulations, are not explicitly incorporated into the governing equations, as discussed by Alpak et al. 2016 and Sussman et al. 2000. Level set methods can accurately capture interface geometry and local fluid properties; however, they generally exhibit weaker mass conservation compared with other approaches, as reported by Sussman et al. 1994 and Sun et al. 2010. Although modified level set techniques, such as two-stage level set methods, have been proposed to improve mass conservation, they are often computationally inefficient, as noted by Olsson et al. 2005 and Olsson et al. 2007.

The phase-field method can effectively preserve mass conservation while accurately capturing interface curvature, particularly in porous media with complex geometries. The Cahn–Hilliard equations ensure mass conservation and can be implemented in both two-dimensional and three-dimensional domains. When coupled with the Navier–Stokes equations, they provide a robust framework for simulating pore-scale two-phase flow, as demonstrated by van der Waals 1979, Cahn et al. 1958, Jacqmin 1999, Chiu 2011, and Bogdanov 2010. The phase-field method is physically based and relies on a free energy functional to describe fluid interfaces, ensuring that the total energy of the system is minimized and that the interface adopts a stable configuration, as discussed by Alpak et al. 2016 and Badalassi et al. 2003. Moreover, rock wettability is directly incorporated into the formulation through boundary conditions applied at the pore walls, enabling the investigation of complex flow regimes such as near-miscible flow, emulsions, and foam flow, as reported by Yue et al. 2006. Owing to these advantages, the phase-field method is adopted in this study to simulate two-phase flow at the pore scale.

Before presenting the methodology of the phase-field approach in detail, it is useful to review selected applications reported in the literature. Zhu et al. 2017 investigated enhanced oil recovery using CO₂ injection at the pore scale in a heterogeneous artificial medium. They demonstrated the applicability of the phase-field method under assumptions including constant gas injection velocity at the inlet, constant outlet pressure, isothermal conditions, and pressure-independent fluid viscosity and density, while neglecting gravitational effects. Basirat et al. 2017 conducted pore-scale simulations to study wettability effects on CO₂–brine displacement during geological storage in deep aquifers. Their model assumed incompressible fluids, negligible mass transfer between phases, pressure-independent fluid properties and surface tension, isothermal conditions, and the absence of gravitational forces. Their results showed that wettability plays a significant role in optimizing gas sequestration.

Bakhshian and Hosseini 2019 employed a multiphase lattice Boltzmann model to simulate supercritical CO₂–brine flow, capturing the evolution of the supercritical CO₂ interface with brine and rock surfaces and analyzing the spatial distribution of residual supercritical CO₂ clusters during brine flooding. Rokhforouz and Akhlaghi 2019 investigated the effects of grain size and shape distributions on pore-scale two-phase flow under different wettability conditions in heterogeneous porous media. Using the phase-field method, they showed that variations in pore structure and wettability significantly affect flow patterns and oil trapping. Guo et al. 2019 applied phase-field modeling to study residual oil distributions and enhanced oil recovery processes, demonstrating that wettability, surface tension, and pore structure strongly influence recovery performance. In another study, Ma et al. 2021 performed pore-scale simulations of CO₂–oil flow in heterogeneous porous media under various conditions. Using

a two-dimensional geometry composed of randomly distributed circular grains, they applied the phase-field method to investigate different miscibility conditions and showed that increasing gas injection rates enhance oil recovery during immiscible displacement.

2.1. Phase field approach in two-phase flow modeling

In the phase-field approach, rather than representing the interface between two fluids as a sharp boundary, the interface is modeled as a thin layer with a finite thickness over which interfacial forces are smoothly distributed, as described by Jacqmin et al. 1999, Chiu et al. 2011, and Bogdanov et al. 2010. This approach focuses on variations in physical properties, such as density and viscosity, across the phase interface, as well as on the effects of interfacial tension and gravity. The interface between the two phases is described using a convection–diffusion equation known as the Cahn–Hilliard equation, as reported by Yue et al. 2004. Within this framework, a phase-field parameter, denoted by ϕ , is introduced to distinguish the two fluid phases and the interfacial region. This parameter assumes constant values within the bulk of each phase and varies smoothly across the interfacial layer.

In a two-phase flow problem, this parameter represents the relative concentration of each fluid at a given point, such that the volume fractions of the first and second phases are given by $\frac{1+\phi}{2}$ and $\frac{1-\phi}{2}$, respectively. Accordingly, the fluid density and viscosity are expressed as $\rho = \rho_{CO_2} \frac{1+\phi}{2} + \rho_o \frac{1-\phi}{2}$ and $\mu = \mu_{CO_2} \frac{1+\phi}{2} + \mu_o \frac{1-\phi}{2}$, respectively. In this approach, the interface between the two fluids is modeled using a free energy density formulation, as given by Equation 1.

$$F(\phi) = \int_{\Omega} \left\{ \frac{1}{2} \lambda |\nabla \phi|^2 + f_o(\phi) \right\} dx \quad (1)$$

where Ω denotes the spatial domain occupied by the two fluids. The first term in this integral represents the surface energy at the fluid–fluid interface, while the second term corresponds to the bulk free energy of the two fluids. The expression $f_o(\phi)$ shown in Equation 2 is defined in terms of two parameters, λ , which represents the mixing energy density, and ϵ , which characterizes the thickness of the capillary interface. These parameters are directly related to the interfacial tension between the fluids, as discussed by Badalassi et al. 2003.

$$f_o(\phi) = \frac{\lambda}{4\epsilon^2} (\phi^2 - 1)^2 \quad (2)$$

Finally, the chemical potential of the system, ξ , can be evaluated using Equation 3.

$$\xi(\phi) = \frac{\delta F(\phi)}{\delta \phi(x)} = -\lambda \nabla^2 \phi(x) + f'_o(\phi(x)) \quad (3)$$

Where ρ is fluid density, μ indicates fluid viscosity, $\xi(\phi)$ is chemical potential, u denotes velocity vector, γ is mobility parameter, χ indicates the adjusting parameter, V_{fi} represents the volume fraction of the fluid, Θ is the contact angle, γ_{sw} is interfacial tension, V denotes the volume of element, S_i indicates oil saturation, K_{effi} is the effective permeability, and K_{ri} denotes relative permeability.

The interface between the two phases becomes stable when the integral of the function ϕ is minimized, resulting in a zero value for the chemical potential, $\xi(\phi)$. In this framework, Cahn and Hilliard considered the gradient of the chemical potential to be proportional to the rate of mass transport within

the system. Consequently, from Equation 4, the changes in the phase-field parameter at the interface between the two fluids can be evaluated.

$$\frac{\partial \varphi}{\partial t} + u \cdot \nabla \varphi = \nabla \cdot [\gamma \nabla (\xi)] = \gamma \lambda \nabla^2 \left[-\nabla^2 \varphi + \frac{\varphi(\varphi^2 - 1)}{\varepsilon^2} \right] \quad (4)$$

Here, u is the velocity vector, and γ is the mobility parameter, which is related to the interface thickness, ε , through the adjusting parameter χ , defined as $\chi = \gamma/\varepsilon^2$. To investigate the dynamics of fluid flow, the continuity equation, $\nabla \cdot u = 0$, is employed together with the Navier-Stokes equation, including an additional term associated with the phase-field parameter, as presented in Equation 5, which accounts for the surface tension forces.

$$\rho(\varphi) \left(\frac{\partial u}{\partial t} + u \cdot \nabla u \right) = -\nabla \cdot [pI + \mu(\varphi)(\nabla u + \nabla u^T)] + \xi(\varphi) \nabla \varphi \quad (5)$$

The density and viscosity are functions of the phase-field parameter through the volume fraction of the fluid, V_{fi} , as defined in Equation 6. When φ equals 1 or -1 , the point is not located within the interface and resides entirely within the bulk of either the first or second fluid.

$$V_{f2} = \frac{1+\varphi}{2} \quad V_{f1} = \frac{1-\varphi}{2} \quad (6)$$

2.2. Determination of relative permeability from pore-scale flow simulation

The relative permeability provides critical information regarding rock and fluid properties, including the wettability of the medium and the critical and residual phase saturations, making it an essential input for flow simulators. Relative permeability curves can be determined using either steady-state or unsteady-state methods. Both approaches can be applied in laboratory experiments on core plug samples to obtain the relative permeability curves. However, laboratory-based determination of relative permeability is generally time-consuming and costly. An alternative approach is to employ pore-scale flow simulations to estimate relative permeability curves. Techniques such as the volume-of-fluid, level-set, and phase-field methods for two-phase flow simulations, combined with the JBN method or the constant pressure approach, have been proposed for this purpose.

Xu et al. (2011) performed three-dimensional two-phase flow simulations using the JBN method to calculate CO₂/water relative permeability. In their study, CO₂ was injected into a medium initially saturated with water, and at various simulation time steps, the gas saturation (S_g), the fraction of water in the outlet flow (f_w), and the injected pore volume were recorded to calculate the relative permeability of each phase. However, comparison of the simulated relative permeability curves with laboratory unsteady-state test results (i.e., the JBN method) revealed poor agreement, particularly for the gas relative permeability curve. This discrepancy was attributed to the inability of the Navier-Stokes equations alone to accurately track fluid interfaces and account for surface tension forces.

He et al. (2019) addressed this limitation by employing the volume-of-fluid approach instead of using the Navier-Stokes equations alone to model the CO₂ drainage process in water-saturated porous media. This approach enables accurate representation of the fluid interface and consideration of wettability effects. In their simulations, a constant CO₂ injection rate was applied at the inlet, and a constant atmospheric pressure was maintained at the outlet. At different time steps, the injected fluid volume, CO₂ saturation, and fraction of water in the outlet flow were recorded, and the JBN method was used to calculate the relative permeability of the two phases. Their results demonstrated that increasing

interfacial tension and decreasing contact angles led to a decrease in water relative permeability and an increase in CO₂ relative permeability.

In 2015, Liu et al. simulated CO₂ flooding using a pore-scale model reconstructed from micro-CT images of a Berea sandstone core to determine two-phase relative permeability curves. A constant pressure difference was applied across the medium. A single-phase simulation was first conducted to determine the total output flow rate, followed by two-phase flow simulations under the same boundary conditions. At each time step, phase saturations and the fraction of each phase in the outlet flow were recorded. Relative permeability was then calculated as the ratio of two-phase to single-phase flow rates and compared with phase saturation at each time step. Their results showed good agreement between pore-scale simulations and laboratory-derived relative permeability curves.

More recently, Song et al. (2023) employed pore-scale numerical simulations using the phase-field method to investigate CO₂–oil displacement and analyze phase relative permeability. They used synthetic porous media composed of circular grains randomly distributed to study the influence of capillary number, viscosity ratio, wettability, density, gravity, interfacial tension, and absolute permeability on flow properties.

Most previous studies on pore-scale numerical simulation of CO₂–oil two-phase flow have focused on simple synthetic porous media composed of randomly distributed circular grains, often assuming constant fluid properties such as viscosity and density. However, these assumptions can significantly affect flow behavior, including two-phase CO₂–brine relative permeabilities. Therefore, in the present study, flow simulations are conducted using realistic porous media extracted from micro-CT images, while accounting for the dependence of fluid viscosity and density on temperature and pressure.

3. Model description

In this study, realistic porous media were employed by selecting two-dimensional images obtained from micro-CT imaging, each representing a square region with a side length of 500 μm. These images provide detailed information about the internal pore structure, including pore connectivity and pore wall roughness. The first step in image analysis involved applying a threshold to the grayscale micro-CT images to separate the porous medium into solid grains and pore space, a process known as binarization. Subsequent steps for simulation were carried out in COMSOL. The grain boundaries of the binary image were extracted and recorded using the “image to curve” function.

To accurately capture the complex pore structure of the binarized image, an unstructured mesh was employed. In this study, triangular elements were used, as they are capable of representing the intricate geometries of the pore space, as illustrated in Figure 1. To model the physics of two-phase displacement, particularly in narrow throats and near rough surfaces, sufficiently small elements were employed. Additionally, because the effects of wettability are a focus of this study, the type and size of mesh elements at pore boundaries in contact with the two phases were carefully chosen to accurately capture changes in wettability.

As mesh resolution critically affects both computation time and the accuracy of simulation results, a sensitivity analysis was conducted to identify a mesh design that is both computationally efficient and capable of providing reliable simulation outcomes.

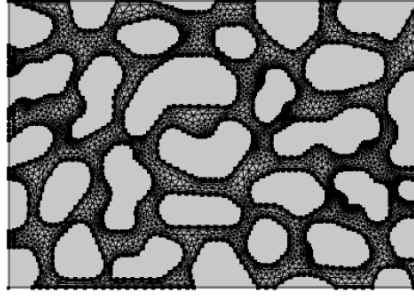


Figure 1

Illustration of the triangular mesh design on a micro-CT image representing a porous medium

To simulate two-phase CO₂/oil displacement in porous media, the phase-field equations described by Cahn and Hilliard were coupled with the Navier-Stokes equations. For the initial conditions, the medium was assumed to be fully saturated with the oil phase at a temperature of 343 K, a pressure of 1500 Pa, and zero velocity at the pore walls (i.e., no-slip flow). No-flow boundary conditions were applied at the upper and lower boundaries of the medium. CO₂ was injected from the left boundary at a rate of 0.01 m/s, while a constant pressure equal to the initial pressure was imposed at the right boundary. It should be noted that the results of phase-field simulations are highly sensitive to the boundary conditions, and this study focuses on small-scale flow features observable at the pore scale, which may not be apparent at larger scales, such as the reservoir scale.

Numerical simulations were performed using the phase-field module of COMSOL, which is based on the finite element method. An initial time step of $\Delta t = 10^{-9}$ s was used and subsequently adapted by the software using a backward differentiation formula as the simulation progressed. A convergence tolerance of 0.001 was applied. The mobility adjusting parameter was set to $\chi = 0.5$ ms/kg, and the interface thickness, ε , was defined as one-quarter of the largest mesh element size.

In most previous studies, fluid density (ρ) and viscosity (μ) were assumed constant, an assumption that may be inaccurate, particularly for CO₂ flooding. In this study, the density and viscosity of CO₂ were modeled as functions of pressure and temperature using the correlations presented in Equation 7, where the parameters c and A are functions of temperature (Ouyang, 2011).

$$\mu(T, p) = C_0 + C_1p + C_2p^2 + C_3p^3 + C_4p^4, \quad \rho(T, p) = A_0 + A_1p + A_2p^2 + A_3p^3 + A_4p^4 \quad (7)$$

In previous simulation studies of carbon dioxide flooding, interfacial tension and wettability were often assumed to be constant. However, experimental studies have demonstrated that both parameters depend on pressure and temperature (Pereira et al., 2016). In the present work, the interfacial tension–pressure data reported by Choudhary et al. for the decane–CO₂ system at $T = 343$ K were employed. A regression analysis was performed to determine the interfacial tension–pressure relationship, as expressed in Equation 8.

$$\sigma = 14.43 - 0.1128p + 4.446 \times 10^{-5}p^2 + 7.967 \times 10^{-7}p^3 \quad (8)$$

The contact angle, representing wettability, was modeled using the correlation provided by Arif et al., which accounts for its dependence on pressure and temperature, as expressed in Equation 9.

$$\cos\theta(p, T) = 1 - 2 \sqrt{\frac{\gamma_{sw}(T)}{\gamma_{cw}(p, T)}} \left[1 - \beta (\gamma_{cw}(p, T) - \gamma_{sw}(T))^2 \right] \quad (9)$$

Here, θ is the contact angle, γ_{sw} is the oil/CO₂ interfacial tension, and γ_{sw} is the surface tension between the oil and the pore wall. The parameters β and γ_{sw} are considered constant across different lithologies and temperatures. Equations 8 and 9 were then coupled with the phase-field modeling equations to incorporate the effects of interfacial tension and wettability.

To validate the assumptions and the numerical simulation model, a single-phase simulation was first performed using the laminar flow module. From this simulation, the porosity and permeability of the medium, as well as the primary flow pathways (i.e., the backbone) within the porous medium, were determined, as shown in Figure 2.

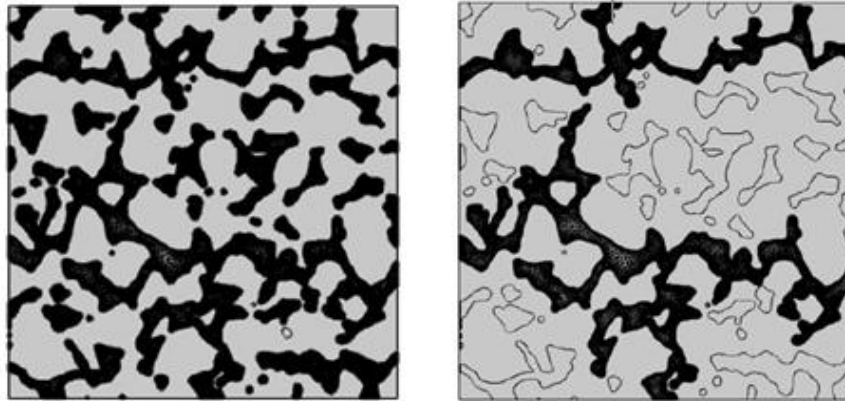


Figure 2

Illustration of (left) the total pore space and (right) the primary flow pathways (i.e., backbone) of the porous medium

A constant pressure was applied at the left boundary, and a fixed pressure difference across the medium ($\Delta p = 1$ Pa) was imposed. The velocity at the right boundary was measured by integrating along the boundary. Using Darcy's law under steady-state flow conditions, the absolute permeability of the system was then calculated. The porosity of the medium was determined as the ratio of the total area covered by the mesh elements (Figure 2) to the total area of the porous medium. Additionally, the effective porosity was defined as the ratio of the area of mesh elements within the flow-carrying part of the medium (Figure 2) to the total porous medium area.

For two-phase flow simulations, the phase-field module of COMSOL was employed. Since only the flow-carrying portion of the medium contributes to displacement, mesh design and flow calculations were restricted to this region. For the base-case model, the interfacial tension was set to $\sigma = 0.004$ N/m, the contact angle to $\theta = 60^\circ$, and the injection rate to $v = 0.01$ m/s. The effects of miscibility were investigated under near-miscible ($\sigma = 0.00004$ N/m) and fully miscible ($\sigma = 0$) conditions. Wettability effects were assessed using contact angles of $\theta = \pi/4$, $\pi/3$, and $\pi/2$. The impact of injection rate was evaluated using two values, $v = 0.01$ m/s and $v = 0.05$ m/s.

Oil recovery was calculated by recording the fluid volume, defined as $\sum V_i \cdot S_i$ where V is the volume of element i and S_i is the oil saturation in element i , as a function of time. Breakthrough time was determined by monitoring the average gas fraction in the outlet flow. To analyze pore-space connectivity, Haines jump diagrams were generated, showing sudden changes in the two-phase pressure difference as a function of injected fluid saturation. These jumps occur when the non-wetting phase pressure must increase sufficiently to overcome the capillary pressure and enter small pores (Zacharoudiou et al., 2018; Anderson, 1987). For this analysis, phase saturations and the pressure difference between the wetting and non-wetting phases were recorded at each time step.

As noted previously, both steady-state and unsteady-state methods can be used to determine relative permeability curves. Unsteady-state methods, such as the JBN method, are often preferred because they are computationally more time-efficient than steady-state methods, which require equilibrium at each step. Most prior pore-scale simulations of two-phase flow used the volume-of-fluid algorithm combined with the JBN method or applied a constant pressure difference. However, the phase-field model, as emphasized earlier, efficiently captures the interface between two phases, making it a more suitable algorithm. Therefore, in this study, the phase-field method was used to determine relative permeability curves.

Steady-state flow simulation conditions were applied to investigate two-phase flow at the pore scale. The porous medium was initially saturated with the first fluid (oil), and CO₂ was injected at the left boundary at a constant rate. Fluid injection continued until the pressure difference across the medium stabilized, indicating steady-state conditions. Subsequently, the volume fraction of the first phase in the injection line was increased by 5% at each simulation stage, resulting in twenty stages for a complete cycle, with the first phase reaching 100% in the final stage. At each stage, simulations were continued until steady-state conditions were achieved, after which fluid saturations, the pressure difference across the medium (Δp), and the flow rate of each phase at the right boundary (Q_i) were recorded. Finally, effective permeability and relative permeability at different fluid saturations were calculated using Equation 10.

$$K_{eff,i} = \frac{Q_i \mu_i L}{A \Delta p}, \quad K_{r,i} = \frac{K_{eff,i}}{K} \quad (10)$$

4. Results and discussion

In this section, the results of relative permeability curves obtained from steady-state pore-scale simulations of CO₂/oil displacement using the phase-field method are presented. In particular, the influence of wettability on two-phase flow behavior and relative permeability curves is examined. Prior to performing two-phase simulations, the properties of the porous medium were characterized, and sensitivity analyses were conducted to establish the range of simulation outcomes. A single-phase steady-state simulation using the laminar flow module in COMSOL was first performed to determine the permeability, total porosity, and effective porosity of the medium. These properties were found to be $7.53 \times 10^{-13} \text{ m}^2$, 0.332, and 0.195, respectively, in good agreement with the reported values for the core sample.

The effects of mesh type and mesh size, the assumption of constant versus pressure-dependent CO₂ density and viscosity, and the CO₂ injection rate were also analyzed. Based on this analysis, a triangular mesh with appropriately distributed element sizes was selected to ensure accurate and efficient simulations. Accounting for pressure- and temperature-dependent CO₂ density and viscosity resulted in minor differences in oil recovery and Haines jumps at the initial stages of simulation, with more pronounced effects as the simulation progressed (e.g., a 5.5% increase in oil recovery). Two injection rates, 0.01 and 0.05 m/s, and surface tensions of $\sigma = 0.004\text{--}0.004 \text{ N/m}$ were considered for sensitivity analysis. While no direct dependency of oil recovery on injection rate was observed, surface tension significantly influenced recovery.

Phase relative permeability curves describe the flow behavior within the pore space, which is governed by the wettability of the medium and the critical and residual saturations of each phase. Therefore, these curves are essential input data for reservoir studies. The CO₂/oil relative permeability curves obtained from the pore-scale simulations are presented here, and the effects of wettability, surface tension, and the direction of two-phase displacement are analyzed. A base case with a contact angle of $\theta = 60^\circ$

(relative to oil) and a surface tension of 0.004 N/m was established to serve as a reference for comparison with other simulation scenarios.

To investigate the drainage process, the medium was initially saturated with the oil phase (wetting phase), and the injected line was assumed to consist entirely of the non-wetting phase (CO₂). Steady-state conditions were simulated by incrementally increasing the percentage of oil in the injection line at each stage until subsequent changes became negligible.

Relative permeability values at each saturation point were calculated by first obtaining the pressure difference (Δp) across the medium at that stage and then applying Equation 10. To determine relative permeability at additional saturation points, the percentage of oil in the injection line was further increased, and the process of measuring the pressure difference and calculating relative permeability was repeated. The resulting relative permeability curves for the two phases in the base-case simulation are shown in Figure 3.

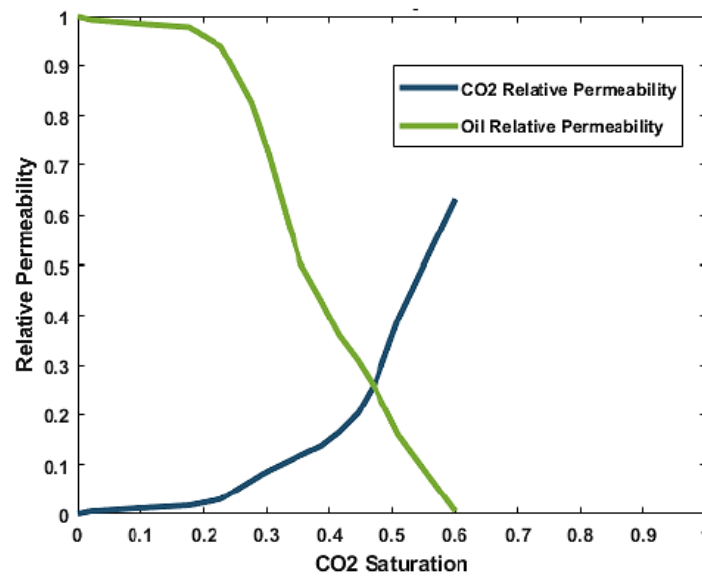


Figure 3

CO₂/oil relative permeability curves for the drainage process in the base case ($\theta = 60^\circ$ and $\sigma = 0.004$ N/m)

As shown in the relative permeability curves (Figure 3), the two curves intersect at $S_{CO_2} = 0.45$ (or $S_{oil} = 0.55$), indicating an oil-wet behavior, which is consistent with the contact angle of $\theta = 30^\circ$ assumed in the simulation and with laboratory observations, where the relative permeability curves typically intersect at $S_{oil} > 50\%$.

Another important parameter for relative permeability curves is the critical saturation (Kumar et al., 2020). As previously noted, the medium is oil-wet, and the saturation above which the CO₂ phase ceases to flow is 60%. Figure 4 illustrates the distribution of the residual oil saturation ($S_{or} = 0.40$) within the medium. One advantage of steady-state simulations is that injection can be continued at each stage until the pressure difference across the medium stabilizes, ensuring that the residual oil saturation remains immobile.

Moreover, the curvature of the relative permeability curves is influenced by the details of flow at the pore scale. For instance, the presence of slip flow affects the shape of these curves. The steady-state pore-scale simulations using the phase-field method presented here are capable of capturing such detailed flow behavior.

In this study, the applicability of the JBN method combined with the phase-field algorithm was also examined for generating CO₂/oil relative permeability curves. However, the results were unsatisfactory. Specifically, when using the JBN method, the relative permeability of the CO₂ phase remained extremely low (approximately 0.00001) for extended simulation times, whereas the oil relative permeability exhibited significant variation. This indicates that the CO₂ phase lacked sufficient mobility within the medium, which was inconsistent with the observed displacement of the injected fluid. Figure 5 illustrates this typical behavior of the CO₂/oil relative permeability curves obtained using the JBN method in conjunction with the phase-field approach.

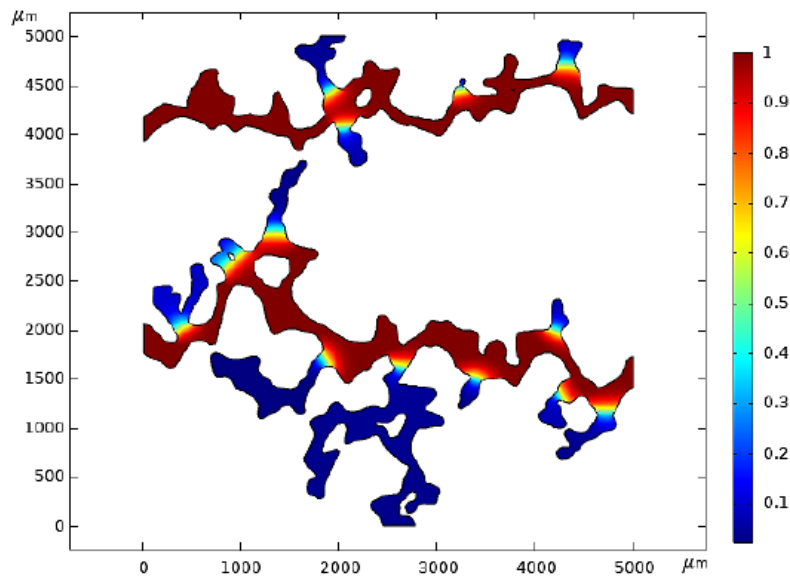


Figure 4

Distribution of residual oil saturation in the medium after CO₂ injection

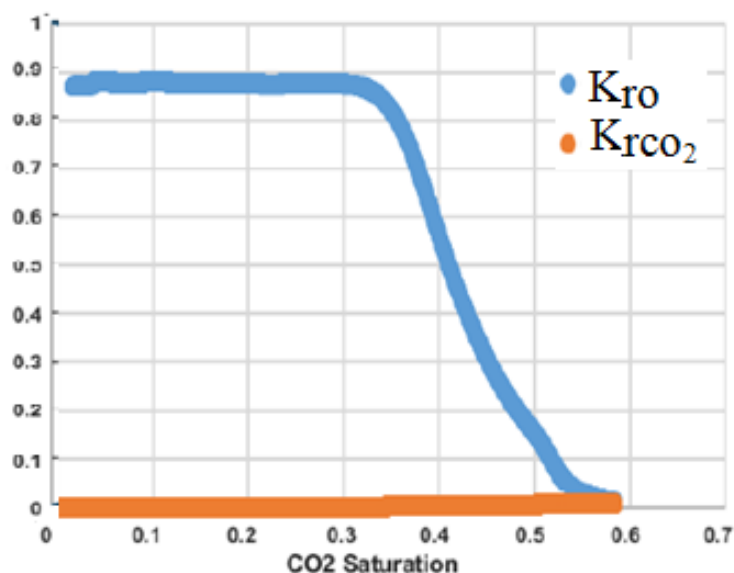


Figure 5

Example of oil/CO₂ permeability curves obtained using the JBN method with the phase-field approach

Additionally, the applicability of the constant pressure method combined with the phase-field algorithm was evaluated for generating relative permeability curves. When applied to a simple artificial porous

medium, this method produced reasonable results for the imbibition process. However, for the drainage process, the relative permeability curves exhibited jumps and irregular behavior. Similar anomalies were observed when this method was applied to a realistic porous medium extracted from micro-CT images. Therefore, for the remainder of this study, focus is placed on steady-state simulations using the phase-field method to generate relative permeability curves.

a) Wettability effects

Although the gas phase is non-wetting, different wettability conditions can be simulated by varying the contact angle in the model. Analysis of Haines jump diagrams during the two-phase displacement process (Figure 6) shows that as the medium becomes more oil-wet, the jumps are more pronounced, indicating increased resistance to fluid entry. Under these conditions, the injected fluid preferentially flows through larger throats and is unable to effectively displace oil from smaller pores and throats.

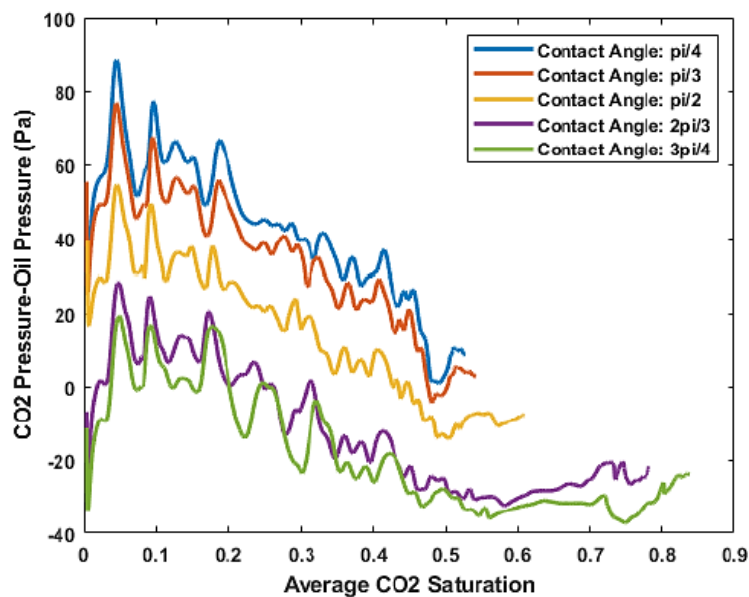


Figure 6

Haines Jump diagram for CO₂ injection process under different wettability conditions

The simulation results also demonstrated an increase of nearly 30% in oil recovery when the contact angle was increased from $\theta = 45^\circ$ to 135° . This behavior is attributed to the stronger tendency of oil-wet media to retain the oil phase along pore surfaces. Because the shape of the relative permeability curves depends on both rock and fluid properties, steady-state simulations were conducted for three contact angle scenarios: $\theta = 60^\circ$, 90° , and 120° . The resulting relative permeability curves for these cases are presented in Figure 7.

As shown in Figure 7, the oil relative permeability increases while the CO₂ relative permeability decreases for cases with larger contact angles. This highlights the greater influence of capillary forces on the displacement process. Such relative permeability behavior under varying wettability conditions has been reported in previous studies (He et al., 2019). Consequently, the displacement efficiency is improved by shifting the intersection point of the relative permeability curves to higher oil saturations, resulting in increased oil recovery, particularly under larger contact angles (i.e., more oil-wet conditions).

A summary of the effects of wettability on the relative permeability curves—including the intersection points, residual/irreducible saturations, and relative permeability endpoints—is presented in Table 1.

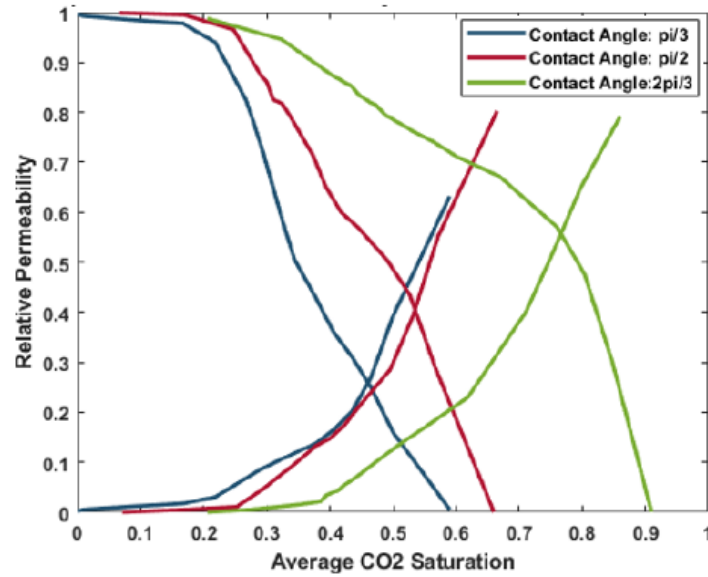


Figure 7

Comparison of relative permeability curves at contact angles $\theta = 60^\circ$ (blue), $\theta = 90^\circ$ (red), and $\theta = 120^\circ$ (green) with surface tension $\sigma = 0.004$ N/m

Table 1

Characteristics of relative permeability diagrams under different wettability conditions

S_{gir}	S_{or}	S_{CO_2} at intersection point	Contact angle
0	0.4	0.45	$\theta=60^\circ$
0.05	0.35	0.52	$\theta=90^\circ$
0.2	0.1	0.76	$\theta=90^\circ$

As observed, for higher contact angles (more gas-wet conditions), the intersection of the relative permeability curves occurs at lower oil saturations (or higher gas saturations), causing the curves to shift toward the right. This behavior is consistent with previous studies on the influence of wettability on relative permeability curves.

b) Surface tension (miscibility) effects

The miscibility between the injected gas and the reservoir fluid can significantly influence two-phase displacement. Figure 8 illustrates the saturation distribution of the injected phase under near-miscible conditions at $t = 0.02$ s. A diffuse transition layer between the two phases is evident, rather than a sharp interface, allowing the injected fluid to more easily penetrate smaller pores.

Furthermore, as miscibility increases, the breakthrough of the injected fluid is delayed, resulting in a longer period for the oil recovery curve to reach a plateau. Figure 9 illustrates the variation of the CO_2 fraction in the outlet flow. In addition, simulations of CO_2 /oil displacement indicate that oil recovery increases by approximately 25% when conditions transition from immiscible to miscible. This improvement is attributed to the enhanced accessibility of smaller pores under miscible conditions.

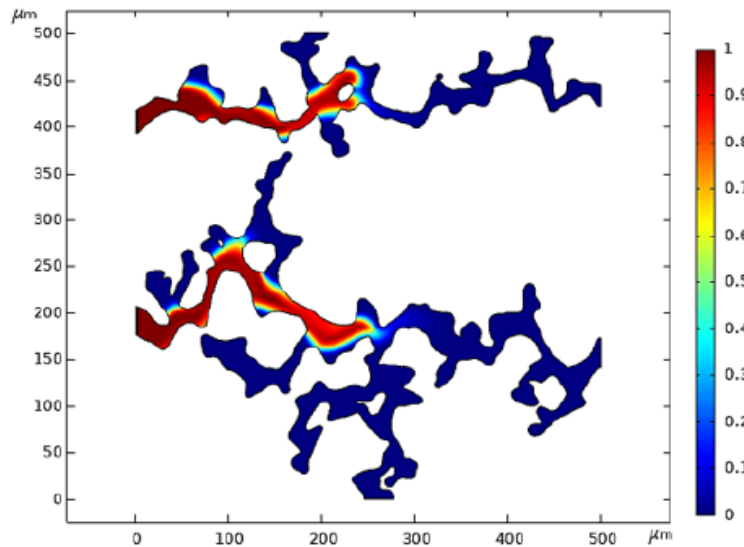


Figure 8

Distribution of injected CO₂ after 0.2 s under slightly miscible conditions

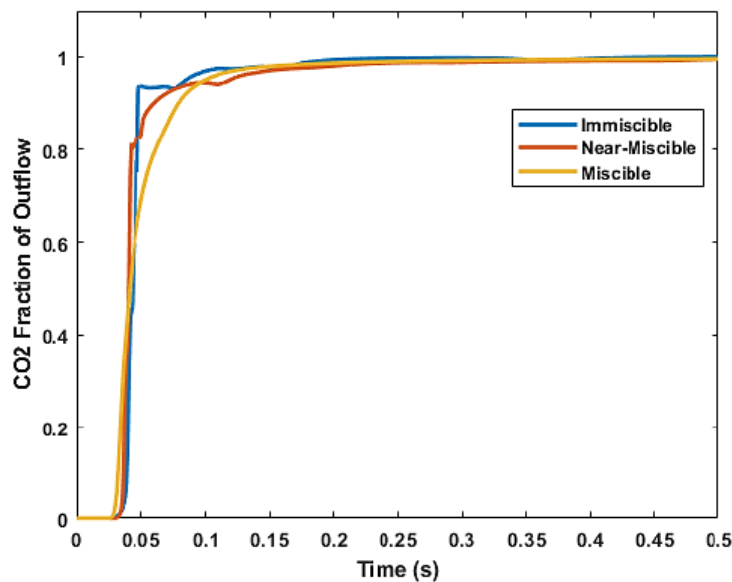


Figure 9

Comparison of CO₂ fraction at the outlet (right boundary) under different miscibility conditions

The effect of surface tension, representing different miscibility conditions, can significantly influence two-phase flow behavior and the resulting relative permeability curves. Figure 10 presents the relative permeability curves obtained from simulations of CO₂/oil displacement using surface tension values of 0.004, 0.0004, and 0.00004 N/m, while maintaining a constant wettability condition ($\theta = 60^\circ$).

As shown, the irreducible saturation of the wetting phase (oil) decreases as surface tension is reduced or miscibility is increased. The relative permeabilities of both oil and CO₂ phases increase with decreasing surface tension, indicating enhanced mobility of both phases due to reduced adhesion to the pore walls. This behavior is attributed to the corresponding increase in the capillary number. Consequently, the displacement efficiency improves, shifting the intersection point of the relative permeability curves to higher oil saturations and resulting in increased oil recovery, particularly under

lower surface tension conditions. These findings are consistent with previous studies on the influence of surface tension on relative permeability diagrams (Maaref et al., 2017).

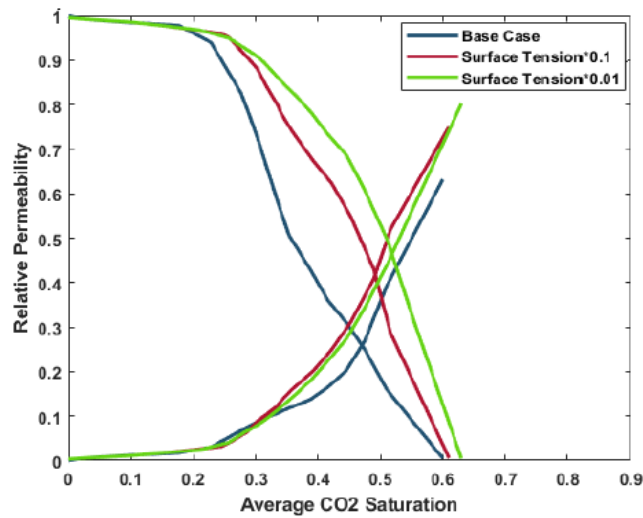


Figure 10

Comparison of relative permeability curves for a fixed wettability condition ($\theta = 60^\circ$) with surface tension values of 0.004, 0.0004, and 0.00004 N/m

Under near-miscible conditions, the relative permeability curves become nearly linear, with the intersection point occurring at $S_{oil} = 50\%$ and a relative permeability value of 0.5, as expected due to the reduced surface tension and weakened capillary forces. A summary of the effects of miscibility on the relative permeability curves—including intersection points, residual/irreducible saturations, and endpoint values—is presented in Table 2.

Table 2

Characteristics of relative permeability curves under different miscibility conditions

S_{or}	S_{CO_2} at intersection point	IFT (N/m)
0.40	0.45	0.004
0.39	0.49	0.0004
0.36	0.52	0.00004

c) Hysteresis effects

The initial saturation distribution in the medium differs between imbibition and drainage processes, resulting in variations in the magnitude of capillary forces and their influence on displacement. Consequently, the wetting and non-wetting phases follow different flow paths within the medium; for example, the wetting phase preferentially moves through smaller pores (Anderson, 1987).

In this section, the same porous medium with identical structural features was used, but the initial condition for imbibition simulations was set as the saturation distribution at the end of the drainage process. This approach allowed the determination of phase relative permeabilities during imbibition. Simulations were conducted for contact angles of $\theta = 60^\circ$, 90° , and 120° to evaluate the effects of wettability on displacement pathways. Figure 11 illustrates the relative permeability curves obtained for both imbibition and drainage processes from the pore-scale flow simulations.

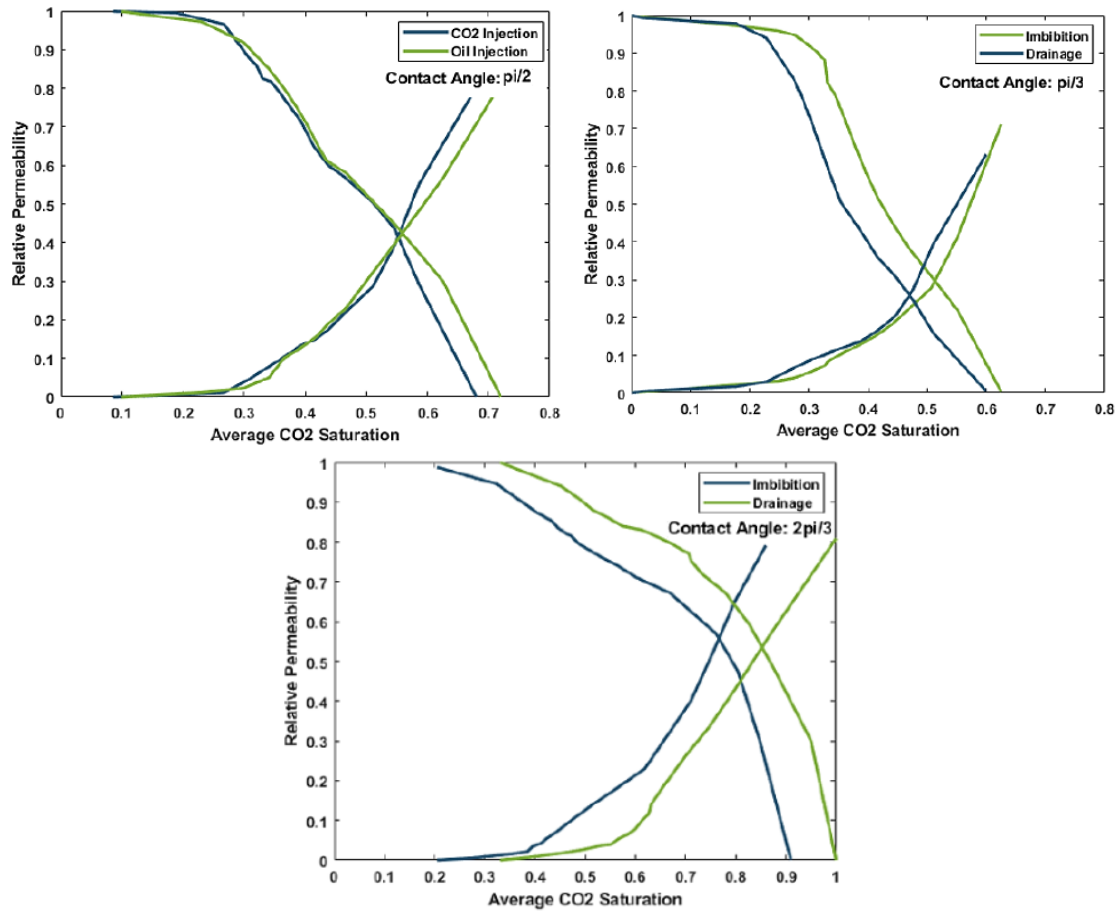


Figure 11

Illustration of relative permeability curves for imbibition and drainage processes at contact angles $\theta = 60^\circ$, $\theta = 90^\circ$, and $\theta = 120^\circ$

As shown in Figure 11, the two-phase relative permeability curves differ between the imbibition and drainage processes. For a contact angle of $\theta = 60^\circ$, a significant deviation is observed in the oil relative permeability curve, whereas for $\theta = 120^\circ$, deviations are evident in both the oil and CO₂ relative permeability curves. These differences arise from variations in capillary forces, which cause the fluids to follow different flow paths during drainage and imbibition under varying wettability conditions. In contrast, for neutral wettability ($\theta = 90^\circ$), the relative permeability curves for imbibition and drainage are nearly identical. Therefore, the gap between imbibition and drainage curves—representing hysteresis effects—becomes more pronounced as the wettability shifts toward larger contact angles. Additionally, the residual oil saturation is higher in the drainage process compared with the imbibition process.

5. Conclusions

Modeling multiphase flow at the pore scale using the phase-field method allows for the incorporation of pressure-dependent fluid properties, enabling more realistic assumptions in flow simulations. The results demonstrate the successful application of the phase-field method to model two-phase flow in geometrically complex media representing real rocks. Wettability influences the role of capillary forces and affects fluid distribution within the medium, leading to corresponding changes in the relative permeability curves. As wettability shifts toward the injected fluid, the Haines jump diagrams become

flatter, the interface between oil and CO₂ becomes less sharp, and the transition zone between the two phases thickens.

The steady-state method combined with the phase-field approach provides a suitable framework for determining CO₂/oil relative permeability curves from pore-scale simulations. This methodology captures the effects of surface tension and wettability and differentiates between imbibition and drainage processes. Specifically, the intersection point of the relative permeability curves shifts to higher oil saturations, resulting in increased oil recovery, particularly at larger contact angles and lower surface tensions. The phase relative permeability curves for imbibition and drainage processes converge under neutral wettability conditions, whereas the gap between these curves—representing hysteresis effects—becomes more pronounced as wettability favors larger contact angles. Additionally, residual oil saturation increases in drainage simulations compared with imbibition cases.

Generalizing the 2D simulation results obtained in this study to 3D structures, based on the steady-state flow and phase-field approach, will provide valuable insights for real-field applications, which are the focus of future research. Furthermore, extending this approach to CO₂ injection in saline aquifers, including the potential effects of chemical reactions, solid particle transport, and porosity changes, can broaden the applicability of the presented methodology.

Nomenclature

φ	Phase field parameter
ρ	Fluid density
μ	Fluid viscosity
ξ	Chemical potential
u	Velocity vector
γ	Mobility parameter
χ	Adjusting parameter
V_{fi}	Volume fraction of the fluid
Θ	Contact angle
γ_{sw}	Interfacial tension
V	Volume of element
S_i	Oil saturation
K_{effi}	Effective permeability
K_{ri}	Relative permeability
λ	Size of mixing energy
ε	Capillary interface thickness

References

- Ajayi T., Gomes J.S., and Bera A., A review of CO₂ storage in geological formations emphasizing modeling, monitoring and capacity estimation approaches, *Petroleum Science*, Vol. 16, No. 5, 2019.
- AkhlaghiAmiri H. A. and Hamouda A.A., Pore-scale modeling of non-isothermal two-phase flow in 2D porous media: Influences of viscosity, capillarity, wettability, and heterogeneity, *International Journal of Multiphase Flow*, Vol. 61, 2014.

- Alpak F.O., Riviere B., and Frank F., A phase-field method for the direct simulation of two-phase flows in pore-scale media using a non-equilibrium wetting boundary condition, *Computational Geosciences*, Vol. 20, No. 5, 2016.
- Alvarado V., and Manrique E., Enhanced oil recovery: An updated review, *Energies*, Vol. 3, No. 9, 2010.
- Anderson W.G., Wettability literature survey-part 5: the effects of wettability on relative permeability, *JPT, Journal of Petroleum Technology*, Vol. 39, No. 11, 1987.
- Arif M., Barifcani A., and Iglauer S., Solid/ CO₂ and solid/water interfacial tensions as a function of pressure, temperature, salinity, and mineral type: Implications for CO₂-wettability and CO₂ geostorage, *International Journal of Greenhouse Gas Control*, Vol. 53, 2016.
- Badalassi V.E., Cenicerros H.D., and Banerjee S., Computation of multiphase systems with phase field models, *Journal of Computational Physics*, Vol. 190, No. 2, 2003.
- Basirat F., Yang Z., and Niemi A., Pore-scale modeling of wettability effects on CO₂-brine displacement during geological storage, *Advances in Water Resources*, Vol. 109, 2017.
- Blunt M. J. et al., Pore-scale imaging and modeling, *Advances in Water Resources*, Vol. 51, 2013.
- Blunt M.J., Jackson M.D., Piri M., and Valvatne P.H., Detailed physics, predictive capabilities and macroscopic consequences for pore-network models of multiphase flow, *Advances in Water Resources*, Vol. 25, No. 8–12, 2002.
- Bogdanov I., Jardel S., Turki A., and Kamp A., Pore-scale phase field model of two-phase flow in porous medium, *Annual COMSOL Conference, Paris, France*, 2010.
- Cahn J.W., and Hilliard J.E., Free energy of a nonuniform system. I. Interfacial free energy, *The Journal of Chemical Physics*, Vol. 28, No. 2, 1958.
- Chiu P.H., and Lin Y.T., A conservative phase field method for solving incompressible two-phase flows, *Journal of Computational Physics*, Vol. 230, No. 1, 2011.
- Choudhary N., NarayananNair A. K., et al., Bulk and interfacial properties of decane in the presence of carbon dioxide, methane, and their mixture, *Scientific Reports*, Vol. 9, No. 1, 2019.
- Christensen J.R., Stenby E.H., and Skauge A., Review of WAG field experience, *SPE Reservoir Evaluation and Engineering*, Vol. 4, No. 2, 2001.
- Ferrari A., Jimenez-Martinez J., et al., Challenges in modeling unstable two-phase flow experiments in porous micromodels, *Water Resources Research*, Vol. 51, No. 3, 2015.
- Flannery B.P., Deckman H.W., et al., Three-dimensional X-ray microtomography, *Science*, Vol. 237, No. 4821, 1987.
- Ghedan S., *Global laboratory experience of CO₂-EOR flooding*, 2020.
- Guo Y. et al., A pore-scale investigation of residual oil distributions and enhanced oil recovery methods, *Energies*, Vol. 12, No. 19, 2019.
- He D., Jiang P., et al., Pore-scale CFD simulation of supercritical carbon dioxide drainage process in porous media saturated with water, *Energy Sources, Part A: Recovery, Utilization and Environmental Effects*, Vol. 41, No. 15, 2019.

- Hemmati-Sarapardeh A., Ghazanfari M.H., Ayatollahi S., and Masihi M., Accurate determination of the CO₂ crude oil minimum miscibility pressure of pure and impure CO₂ streams: A robust modelling approach, *The Canadian Journal of Chemical Engineering*, Vol 94, p. 253–261, 2016.
- Herring A.L., Harper E.J., Andersson L., et al., Effect of fluid topology on residual nonwetting phase trapping: Implications for geologic CO₂ sequestration, *Advances in Water Resources*, Vol. 62, 2013.
- Hirt C.W. and Nichols B.D., Volume of fluid (VOF) method for the dynamics of free boundaries, *Journal of Computational Physics*, Vol. 39, No. 1, 1981.
- Hu R., Wan J., Kim Y., and Tokunaga T.K., Wettability effects on supercritical CO₂–brine immiscible displacement during drainage: Pore-scale observation and 3D simulation, *International Journal of Greenhouse Gas Control*, Vol. 60, p. 129–139, 2017.
- Hu H.H., Patankar N.A., and Zhu M.Y., Direct numerical simulations of fluid-solid systems using the arbitrary Lagrangian-Eulerian technique, *Journal of Computational Physics*, Vol. 169, No. 2, 2001.
- Huang W., Moving mesh methods based on moving mesh partial differential equations, *Journal of Computational Physics*, Vol. 113, No. 2, 1994.
- Idowu N.A., and Blunt M. J., Pore-scale modeling of rate effects in waterflooding, *Transport in Porous Media*, Vol. 83, No. 1, 2010.
- Jacqmin D., Calculation of two-phase Navier-Stokes flows using phase-field modeling, *Journal of Computational Physics*, Vol. 155, No. 1, 1999.
- Joekar-Niasar V., Hassanizadeh S.M., and Dahle H.K., Non-equilibrium effects in capillarity and interfacial area in two-phase flow: Dynamic pore-network modeling, *Journal of Fluid Mechanics*, Vol. 655, 2010.
- Kaldi J.G., Gibson-Poole C.M., and Payenberg T.H.D., Geological Input to Selection and Evaluation of CO₂ Geosequestration Sites, *AAPG Studies in Geology*, 2009.
- Kumar M., and Fogden A., Patterned wettability of oil and water in porous media, *Langmuir*, Vol. 26, No. 6, 2010.
- Kumar S., Esmaeili S., Sarma H., and Maini B., Can affects
- Kumar S., Esmaeili S., Sarma H., and Maini B., Can effects of temperature on two-phase gas/oil-relative permeabilities in porous media be ignored? A critical analysis, *Energies*, Vol. 13, No. 13, 2020.
- Li, X., Xue, J., Wang, Y., Yang, W., Lu, J., Experimental study of oil recovery from pore of different sizes in tight sandstone reservoirs during CO₂ flooding. *Journal of Petroleum Sciences and Engineering*, Vol. 208, 2022.
- Liu J. and Song R., Investigation of water and CO₂ flooding using pore-scale reconstructed model based on micro-CT images of Berea sandstone core, *Progress in Computational Fluid Dynamics*, Vol. 15, No. 5, 2015.
- Liu J.J., Song R., and Cui M.M., Improvement of predictions of petrophysical transport behavior using three-dimensional finite volume element model with micro-CT images, *Journal of Hydrodynamics*, Vol. 27, No. 2, 2015.
- Lokhorst A., and Wildenborg T., Introduction on CO₂ geological storage. Classification of storage options, *Oil and Gas Science and Technology*, Vol. 60, No. 3, 2005.

- Ma Q. et al., Pore-scale simulations of CO₂/oil flow behavior in heterogeneous porous media under various conditions, *Energies*, Vol. 14, No. 3, 2021.
- Maaref S., Rokhforouz M. R., and Ayatollahi S., Numerical investigation of two-phase flow in micromodel porous media: Effects of wettability, heterogeneity, and viscosity, *Canadian Journal of Chemical Engineering*, Vol. 95, No. 6, 2017.
- Manrique E.J., Muci V.E., and Gurfinkel M.E., EOR field experiences in carbonate reservoirs in the United States, *SPE Reservoir Evaluation and Engineering*, Vol. 10, No. 6, 2007.
- Masihi M, and Firoozmand H., Investigation of the effects of miscibility, wettability, injection rate during CO₂ injection in pore scale of reservoir rocks, Vol. 34, p. 49–51, 2024.
- Meakin P., and Tartakovsky A.M., Modeling and simulation of pore-scale multiphase fluid flow and reactive transport in fractured and porous media, *Reviews of Geophysics*, Vol. 47, No. 3. 2009.
- Olsson E., and Kreiss G., A conservative level set method for two-phase flow, *Journal of Computational Physics*, Vol. 210, No. 1, p. 225–246, 2005.
- Olsson E., Kreiss G., and Zahedi S., A conservative level set method for two-phase flow II, *Journal of Computational Physics*, Vol. 225, No. 1, 2007.
- Ouyang L.B., New correlations for predicting the density and viscosity of supercritical carbon dioxide under conditions expected in carbon capture and sequestration operations, *Open Petroleum Engineering Journal*, Vol. 4, No. 1, 2011.
- Pereira L.M.C., Chapoy A., Burgass R., and Tohidi B., Measurement and modeling of high-pressure density and interfacial tension of (gas + n-alkane) binary mixtures, *Journal of Chemical Thermodynamics*, Vol. 97, 2016.
- Piri M., and Blunt M.J., Three-dimensional mixed-wet random pore-scale network modeling of two- And three-phase flow in porous media. I. Model description, *Physical Review E - Statistical, Nonlinear, and Soft Matter Physics*, Vol. 71, No. 2, 2005.
- Popinet S., and Zaleski S., A front-tracking algorithm for accurate representation of surface tension, *International Journal for Numerical Methods in Fluids*, Vol. 30, No. 6, 1999.
- Raeini A.Q., Blunt M.J., and Bijeljic B., Modelling two-phase flow in porous media at the pore scale using the volume-of-fluid method, *Journal of Computational Physics*, Vol. 231, No. 17, 2012.
- Rokhforouz M.R., and AkhlaghiAmiri H.A., Effects of grain size and shape distribution on pore-scale numerical simulation of two-phase flow in a heterogeneous porous medium, *Advances in Water Resources*, Vol. 124, 2019.
- Saraf S., and Bera A., A review on pore-scale modeling and CT scan technique to characterize the trapped carbon dioxide in impermeable reservoir rocks during sequestration, *Renewable and Sustainable Energy Reviews*, Vol. 144., 2021.
- Sethian J.A., and Smereka P., Level set methods for fluid interfaces, *Annual Review of Fluid Mechanics*, Vol. 35, 2003.
- Shi, Y., Tang, G., Non-Newtonian rheology property for two-phase flow on fingering phenomenon in porous media using the lattice Boltzmann method. *Journal of Non-Newtonian Fluid Mechanics*, Vol. 229, p. 86–95, 2016.
- Song R., Tang Y., et al., Pore-scale numerical simulation of CO₂–Oil two-phase flow: a multiple-parameter analysis based on phase-field method, *Energies*, Vol. 16, 2023.

- Spiteri E.J., Juanes R., Blunt M.J. and Orr F.M., Relative permeability hysteresis: trapping models and application to geological CO₂ sequestration, Paper presented at the SPE Annual Technical Conference and Exhibition, Dallas, Texas, October 2005. (SPE-96448-MS)
- Srivastava R.K., Huang S.S., and Dong M., Laboratory investigation of Weyburn CO₂ miscible flooding, *Journal of Canadian Petroleum Technology*, Vol. 39, No. 2, 2000.
- Sun D.L., and Tao W.Q., A coupled volume-of-fluid and level set (VOSET) method for computing incompressible two-phase flows, *International Journal of Heat and Mass Transfer*, Vol. 53, No. 4, 2010.
- Sussman M., A level set approach for computing solutions to incompressible two-phase flow, *Journal of Computational Physics*, Vol. 114, No. 1, 1994.
- Sussman M., and Puckett E.G., A coupled level set and volume-of-fluid method for computing 3D and axisymmetric incompressible two-phase flows, *Journal of Computational Physics*, Vol. 162, No. 2, 2000.
- Teklu T.W., Alameri W., Graves R.M., Kazemi H., and Al-Sumaiti A.M., Low-salinity water-alternating- CO₂ EOR, *Journal of Petroleum Science and Engineering*, Vol. 142, 2016.
- Tryggvason G., et al., A front-tracking method for the computations of multiphase flow, *Journal of Computational Physics*, Vol. 169, No. 2, 2001.
- van der Waals J.D., The thermodynamic theory of capillarity under the hypothesis of a continuous variation of density, *Journal of Statistical Physics*, Vol. 20, No. 2, 1979.
- Wildenschild D., Vaz C.M.P., et al., Using X-ray computed tomography in hydrology: Systems, resolutions, and limitations, *Journal of Hydrology*, Vol. 267, No. 3–4, 2002.
- Xu R., Luo S., and Jiang P., Pore-scale numerical simulation of supercritical CO₂ injecting into porous media containing water, *Energy Procedia*, Vol. 4, p. 4418–4424, 2011.
- Yue P., Zhou C., et al., Phase-field simulations of interfacial dynamics in viscoelastic fluids using finite elements with adaptive meshing, *Journal of Computational Physics*, Vol. 219, No. 1, 2006.
- Yue, P.T., Feng, J.J., Liu, C., and Shen, J., A diffuse-interface method for simulating two-phase flows of complex fluids, *Journal of Fluid Mechanics*, 515, 293–317, 2004.
- Zacharoudiou I., Boek E. S., and Crawshaw J., The impact of drainage displacement patterns and Haines jumps on CO₂ storage efficiency, *Scientific Reports*, Vol. 8, No. 1, 2018.
- Zhang, C., Oostrom, M., Grate, J., Liquid CO₂ displacement of water in a dual-permeability pore network micromodel. *Environmental Sciences Technology* Vol. 45, p. 7581–7588, 2011.
- Zhu G., Yao J., Li A., et al., Pore-scale investigation of carbon dioxide-enhanced oil recovery, *Energy and Fuels*, Vol. 31, No. 5, 2017.

**COPYRIGHTS**

©2023 by the authors. Licensee Iranian Journal of Oil & Gas Science and Technology. This article is an open-access article distributed under the terms and conditions of the Creative Commons Attribution 4.0 International (CC BY 4.0) (<https://creativecommons.org/licenses/by/4.0/>)